Evidence for the physical basis and universality of the elimination of particulates using dual-laser ablation. II. Dynamic time-resolved target reflectivity of metals and film growth of Zn

Pritish Mukherjee,[a] Shudong Chen,[b] John B. Cuff, and Sarath Witanachchi
Department of Physics, Laboratory for Advanced Materials Science and Technology (LAMSAT), University of South Florida, Tampa, Florida 33620

(Received 16 October 2000; accepted for publication 26 November 2001)

We have presented, in Part I of this series of two articles, the applicability of dynamic melt studies of the surface of a target under pulsed CO_2 laser radiation to determine the onset of melt in these targets. Determination of this time and the accurate synchronization of an excimer (KrF) laser to coincide with the onset of melt on the target surface was shown to lead to particulate-free film deposition for Y_2O_3 and ZnO films. A key feature of the pump–probe reflectivity studies was the dynamic enhancement of the reflected probe signal, indicating the onset of melt. Some metallic targets, depending on the diameter of the precursor powder globules, such as the zinc target used in this study, do not yield such observable enhancements. In this article (Part II) we present the determination of the time for ablation of a variety of metallic targets under pulsed CO_2 laser radiation, by monitoring the dynamic target reflectivity. The melt time is either directly determined or, in the absence of observable melt, estimated based on a simple thermal model for the absorption of the laser radiation by the target. Correlation of the calculated melt times with the morphological quality of particulate-free film growth of Zn is demonstrated. The effect of variable CO_2 laser fluence on the deposited films is also demonstrated. The universality of applicability of the target reflectivity studies to a wide range of dissimilar materials, as well as the physical basis for the removal of particulates in dual-laser ablation is established. © *2002 American Institute of Physics.* [DOI: 10.1063/1.1435419]

I. INTRODUCTION

The application of transient reflectivity measurements to low thermal conductivity sintered, pressed-powder targets, under pulsed CO_2 laser irradiation has previously been used to demonstrate the onset of melt in such samples during the laser pulse.[1] In this work,[1] a variety of probing configurations were shown to yield consistent results for the time and energy of melt for Y_2O_3 and ZnO samples, dependent on the fluence of the incident 150 ns CO_2 laser pulse. It was further demonstrated that in the growth of films of both these samples under dual-laser ablation,[1,2] essentially particulate-free films were obtained when the synchronization of the 20 ns KrF laser pulse was such that it spatially overlapped on the target, and arrived at the onset of CO_2 laser-induced melt predicted by the results of the transient reflectivity measurements. This provided direct evidence of the physical mechanism responsible for the elimination of particulates in this film growth process. It also established the validity of the application of transient reflectivity measurements to determine the onset of melt in low thermal conductivity samples. Details of the general characteristics of the particulate problem in thin film growth using laser ablation, previous work directed at elimination of these particulates and a resolution of this problem using dual laser ablation have been discussed in Part I. In this article (Part II) we present the results of the application of dynamic transient reflectivity measurements to several thermally conductive metals, including Mg, Al, and Zn. These experiments probe the universality of the conclusions established in Part I regarding the physical basis of particulate-free film deposition in this system. They also extend the domain of transient target reflectivity measurements for the determination of the time of phase transformations in a variety of materials.

The remainder of the article is organized as follows. In Sec. II we describe the dynamic target reflectivity studies performed on Mg and Al and compare the general characteristics of the observed onsets of melt in the two metals based on their thermal properties. This is followed in Sec. III with experiments performed on a Zn target. A modified transient reflectivity technique and a model for the determination of the onset of melt, based on observation of the onset of ablation in a sample, are presented. These results are verified by the growth of Zn films. The article is concluded in Sec. IV.

II. DYNAMIC TARGET REFLECTIVITY OF Mg AND Al

Three different transient reflectivity measurements were introduced in Part I. Each of these techniques relied on changes in reflectivity of the specularly reflected laser pulse signal from a rough, sintered, pressed powder target under CO_2 laser pumping. In two of these techniques, a strong, high intensity CO_2 laser pump beam was used to produce the phase transformation of the material, while a weak probe

[a]Author to whom correspondence should be addressed; electronic mail: pritish@chuma.cas.usf.edu
[b]Currently at E-TEK Dynamics, 1865 Lundy Avenue, San Jose, CA 95131.

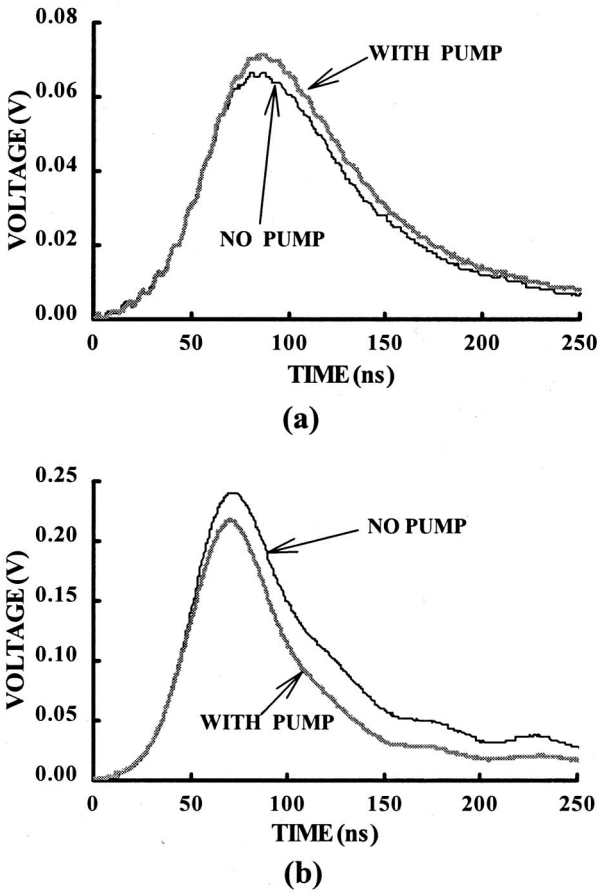

FIG. 1. Transient probe reflectivity with and without the pump pulse for a Mg target at a pump CO_2 laser fluence of: (a) 1.45 J/cm^2 and (b) 2.13 J/cm^2, using the pump–probe with data averaging technique.

beam that had been split from the pump beam was detected by a HgCdTe detector to monitor the surface reflectivity. These included transient probe reflectivity in a standard pump–probe technique with data averaging, and a pump–probe arrangement including a pulse monitor for single-shot detection. The third single-beam technique monitored the transient pump reflectivity. Since all these configurations were shown to provide consistent results for the onset of melt and ablation for Y_2O_3 and ZnO in Part I, the experiments for Mg and Al focused on using only the pump–probe technique including data averaging.

As described in Part I, an orthogonally polarized strong pump–weak probe combination was used to obtain the transient probe reflectivity with a high rejection of the scattered pump. The specularly reflected probe pulses are detected by a fast HgCdTe detector and averaged typically over 32 shots using a digital oscilloscope. By comparing the temporal probe pulse profiles with and without the pump pulse being incident on the sample, the change of target surface reflectivity can be obtained, and hence the time for the onset of melt and ablation. Representative data are shown in Figs. 1 and 2 for packed powder targets of Mg and Al, respectively.

When the Mg target was exposed to the CO_2 pump pulse at a fluence of 1.45 J/cm^2, an increase of the reflectivity can be observed [Fig. 1(a)]. No ablation due to the pump pulse is observed at this laser fluence. With a higher pump fluence

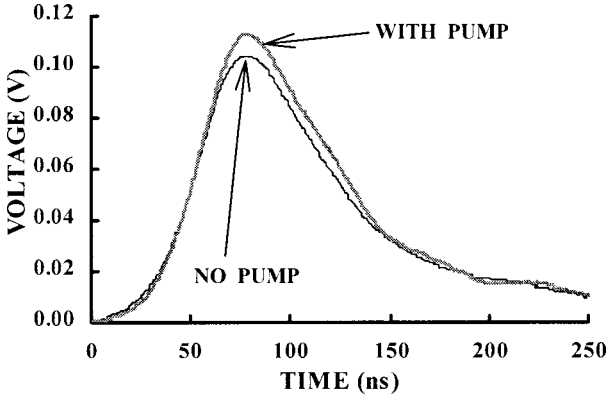

FIG. 2. Transient probe reflectivity with and without the pump pulse for an Al target at a pump CO_2 laser fluence of 2.15 J/cm^2, using the pump–probe with data averaging technique.

(2.13 J/cm^2), the surface reflectivity was observed to decrease [Fig. 1(b)]. This suggests that an increase of pump laser fluence from 1.45 to 2.13 J/cm^2 will cause ablation rather than just melting. The ablation of Mg occurred as early as 48 ns. Thus, 1.45 J/cm^2 is a suitable CO_2 laser fluence for particulate-free thin film deposition of Mg using dual-laser ablation for two reasons. At this fluence, ablation by the CO_2 laser itself is avoided. Also, as shown in Fig. 1(a), the optimum time to introduce the KrF laser for dual laser ablated film growth of Mg can be anywhere between 75 and 150 ns after the onset of the CO_2 laser pulse, thus providing a long time window for interpulse synchronization. Of course, for maximum coupling of the remainder of the CO_2 laser pulse into the KrF laser-generated plasma, the 75 ns time delay is preferable.

The interaction of the CO_2 laser with a packed powder target of Al was studied using CO_2 pump fluences ranging from 0.32 to 3.14 J/cm^2. Of the laser fluences studied, 2.15 J/cm^2 is an appropriate laser fluence for Al thin film deposition. The measured surface reflectivity change is indicated in Fig. 2. The increase of surface reflectivity occurs 60 ns after the onset of CO_2 pulse, and drops back to normal at around 150 ns, with no ablation by the CO_2 laser pulse. As explained earlier for Mg, the KrF laser can be coupled in at any time within this time window, but preferably closer to the 60 ns delay for optimum plume excitation and evaporation of submicron particulates.

Following the results obtained in Part I for Y_2O_3 and ZnO, Figs. 1 and 2 show a similar behavior for Mg and Al. Therefore, particulate-free film growth under the conditions discussed above should be possible. The reliability of this diagnostic technique can also be verified by a simple comparison between Mg and Al. The thermal conductivity of Mg is about 1.5 $W\,cm^{-1}\,K^{-1}$, which is lower than the corresponding value of 2.5 $W\,cm^{-1}\,K^{-1}$ for Al.[3] The heat capacity of Mg is also lower than that of Al.[4] Thus, the melting process for Mg should take place more easily and earlier than for Al. This prediction is verified by Figs. 1 and 2. The Al target melts with no ablation at 2.15 J/cm^2. However, for the case of Mg we observe ablation at the same fluence. Consistent with the previous discussion, Mg exhibits melt at a lower fluence of 1.45 J/cm^2.

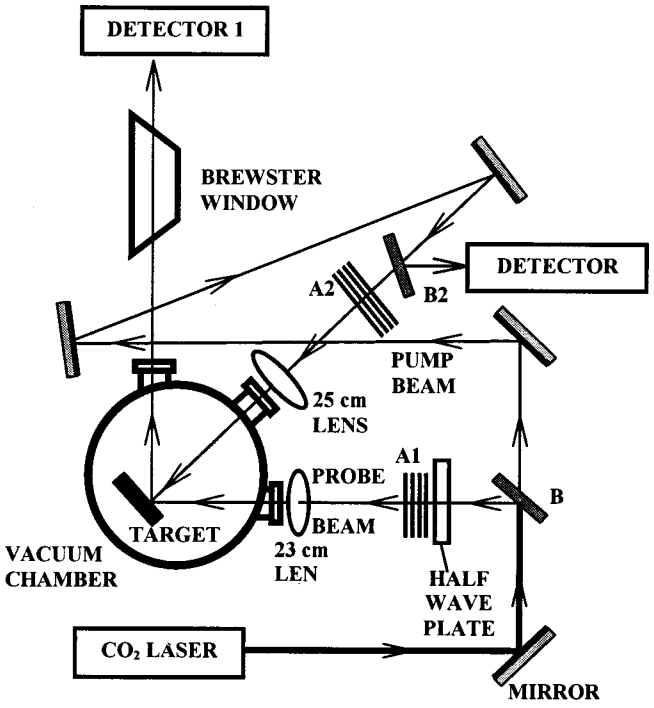

FIG. 3. The experimental setup for transient single-shot reflectivity including a pump beam delay.

III. DYNAMIC TARGET REFLECTIVITY AND FILM GROWTH OF Zn

Experiments were performed using the pump–probe technique for a pressed-powder target of Zn. However, this target showed no evidence of enhanced reflectivity corresponding to melt over a large range of pump CO_2 fluence. We speculated that it might be the consequence of a very early onset of melt at a time when the probe signal was too low to detect the enhancement. In an attempt to overcome this obstacle, we introduced a monitoring technique for low-noise detection of transient reflectivity, by introducing an optical delay of the pump pulse with respect to the probe pulse. The basic idea was to allow the probe intensity to build up prior to incidence of the strong pump pulse on the Zn target. This technique is presented in Sec. III A and then the data are used to obtain the melt times in Sec. III B.

A. Transient single shot reflectivity with beam delay

This technique makes use of the single-shot pump–probe configuration described in Part I. The difference with the standard pump–probe technique was the addition of another detector to monitor the laser pulse shape directly, so that the scattered probe pulse could be compared to the actual laser pulse directly for each individual laser shot. In addition a 37 ns delay for the pump pulse, corresponding to an increased path length of about 11.4 m relative to the probe, was introduced. The entire setup is shown in Fig. 3. The probe pulse arrived first at the target and was detected by a HgCdTe detector. The pump pulse reached the target 37 ns later. The 37 ns delay of the pump pulse was introduced to avoid using the early part of the probe pulse where the signal is lower and therefore the relative reflectivity measurements are prone to noise.

Pressed-powder targets of Zn were prepared starting from 7 μm diam zinc globules obtained from Johnson Matthey. Interaction of the CO_2 laser with the Zn target was studied by using the method of single-shot comparison with pump delay. The basic aim was to determine the time for the onset of melt of the Zn target to enhance the deposition of particle-free Zn films. Experiments were carried out in vacuum to acquire data on Zn that is close to the deposition conditions. CO_2 laser fluences from 1.26 to 13.10 J/cm^2 were used in the experiments. Plume cutoff was detected within the range of CO_2 laser fluences from 5.85 to 13.10 J/cm^2 (Fig. 4).

Despite the introduction of pump delay and evidence for plume emission by probe pulse truncation, an interesting observation in Fig. 4 is the absence of any increased reflectivity due to the onset of melt, unlike the cases for Mg and Al targets discussed earlier. An explanation for this lies in the ingredients used to prepare the packed powder targets in these three cases. The starting granular particle sizes for the Mg and Al powders were 70 μm while that for Zn was 7 μm. This results in a greater compaction and reduced surface roughness for the Zn target in comparison with those for Mg and Al. In particular, for the CO_2 laser wavelength of 10.6 μm, the Zn target is inherently much more reflective. Therefore, upon the onset of melt the relative change in specular reflectivity is negligible compared to the rougher Mg and Al targets, and is thus not observed.

B. A model to find the onset of melt

Thermodynamic models have been used to predict the ablation thresholds of metal (Ni and Au) films based on their optical properties, evaporation enthalpies, and thermal diffusivities.[5] Laser energy absorption leading to heat transfer and considerations relevant to melt modeling for laser ablation have been discussed.[6] Since we do not directly observe the melting of Zn, a simple model was used to determine the time for the onset of melt from the observed time for ablation. In Fig. 4, the area under the recorded intensity profile of the pump pulse is directly proportional to the energy of the pulse. If we assume that the material will undergo a sequence of heating and phase transformation to the molten state, followed by a transformation to the vapor phase for ablation; the proportion of the energy E' used to melt the material, to the energy used to ablate it, can be written as

$$\alpha = \frac{E'}{E' + E'' + m' L_v}, \tag{1}$$

or

$$\alpha = \frac{m\int_{T_0}^{T_m} C_p\, dT + mL_f}{(m\int_{T_0}^{T_m} C_p\, dT + mL_f) + m\int_{T_m}^{T_0} C_p\, dT + m' L_v},$$

$$\alpha = \frac{\int_{T_0}^{T_m} C_p\, dT + L_f}{\int_{T_0}^{T_m} C_p\, dT + L_f + \int_{T_m}^{T_b} C_p\, dT + \beta L_v}, \tag{2}$$

where m is the total mass of the material affected by the CO_2 laser pulse, m' is the mass of the vaporized material, β is the ratio of m' to m, C_p is the specific heat of the material under

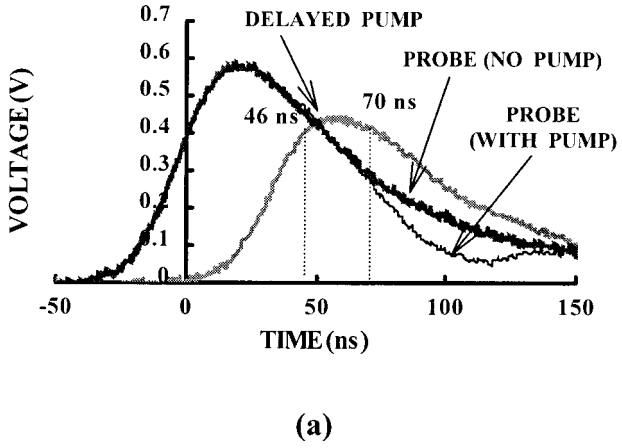

FIG. 4. Time-resolved probe reflectivity for a Zn target in vacuum using the single-shot probing technique including a beam delay. Results are shown at pump CO_2 laser fluences of: (a) 5.85 J/cm^2, (b) 8.57 J/cm^2, and (c) 13.10 J/cm^2. Each trace includes the pump pulse as well as the probe pulse, with and without the pumping of the target.

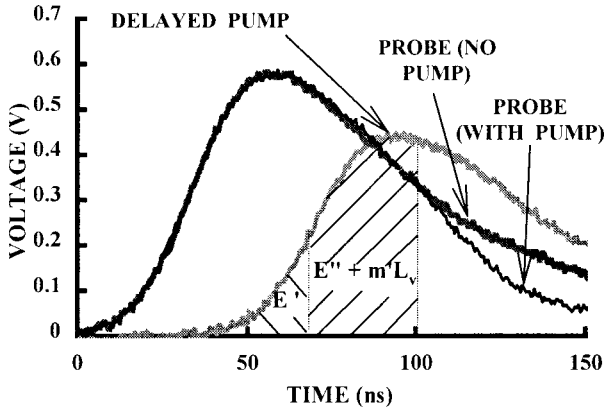

FIG. 5. A representation of the partitioning of the pump pulse based on the ratio of energy required to melt and vaporize the target, respectively.

constant pressure, T_0 is room temperature, T_m is the melting point of the material, T_b is the boiling point of the material, E'' is the energy required to transform the liquid from the melting to the boiling point, L_f is the latent heat of fusion, and L_v is the latent heat of vaporization.

According to the ratio in Eq. (1), the area under the pump pulse can be partitioned into three parts, which are shown in Fig. 5 (for illustration only). The first section (E') represents the energy it takes to melt the material, the second section ($E''+m'L_v$) is the energy used to raise the temperature of the molten zone to its boiling point and vaporize it, while the third section is the laser energy that may be absorbed by the ablated plume. The area in each section can be integrated to get the corresponding energy for that portion of the laser–target interaction.

In order to determine the time for the onset of melt based on the time of ablation, it is necessary to determine the parameter β, which is m'/m. Two physical quantities determine the value of β. The first is the optical penetration depth (also called skin depth) given by

$$\delta = \frac{1}{4\pi}\sqrt{\frac{c\lambda_0}{\mu\sigma}}, \tag{3}$$

where c is the speed of light, λ_0 is the wavelength, μ is the permeability, and σ the electrical conductivity. The second quantity is the thermal diffusion length

$$l_d = \frac{K\Delta T t_m}{F}, \tag{4}$$

where K is the thermal conductivity, ΔT is the temperature gradient, t_m is the time for which the material receives energy from the laser pulse until it starts to vaporize, and F is the laser fluence.

For Zn, the CO_2 laser penetration depth is 11 nm. The diffusion length, according to Eq. (4), is from 29 to 127 nm depending on different laser fluences, and is therefore much larger than the skin depth. When the target is exposed to the laser pulse, the surface material within the skin depth will be heated. At the same time, the laser energy will diffuse deeper into the bulk of the material, thereby creating a temperature gradient from a high surface temperature to room temperature within the bulk of the material. By the time the surface starts to vaporize, the ratio of the vaporized material to the total mass of the heated material can be approximated by δ/l_d, which is the value for β.

The α in Eq. (2) can be calculated if β is known. The heat capacitance of zinc as a function of temperature is given by[7]

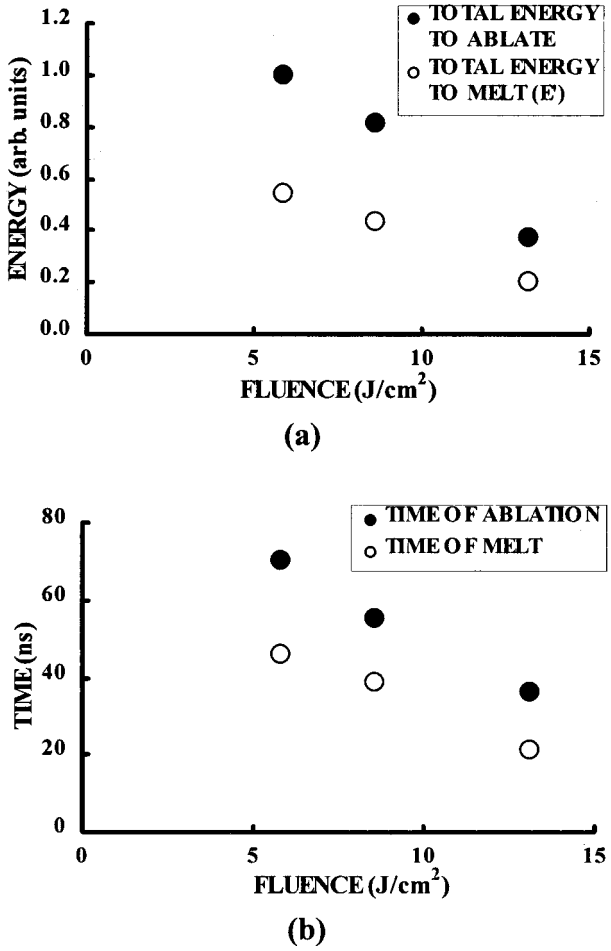

FIG. 6. (a) Normalized energy and (b) calculated time required to melt and ablate the Zn target for various CO_2 laser fluences.

$$C_p = 5.099 + 2.784 \times 10^{-3} T + 0.126 \times 10^{-5} T^{-2}. \quad (5)$$

The melting point T_m for Zn is 692.73 K, the boiling point is 1180 K, the latent heat of fusion L_f is 1.750 K cal/mole, and the latent heat of vaporization is 27.565 K cal/mole. From Eq. (2), α can be calculated to be 0.413, 0.345, and 0.234 for the experimental laser fluences of 5.85, 8.57, and 13.10 J/cm^2, respectively.

The energy needed to ablate the target at different CO_2 laser fluences is shown in Fig. 6(a). These energies were obtained by integrating the areas of the corresponding temporal profiles of the pump pulse up to the onset of ablation in Fig. 4. The energies are measured in arbitrary units as we need only the relative energies in each case for comparative studies. Also, the determination of the melt time requires relative values of E' and $E''+m'L_v$, for Eq. (1), as α is a ratio. The calculated values of α are used, in conjunction with the total energy to ablate Zn to determine the relative energy required to melt the Zn target as a function of laser fluence. This is also shown in Fig. 6(a).

Knowing the energy required to melt Zn for each laser fluence, the temporal profile of the pump pulse could be used from Fig. 4 to determine the time for onset of melt at each laser fluence. The calculated melting times are 46, 39, and 21 ns for incident CO_2 laser fluences of 5.85, 8.57, and 13.10 J/cm^2, respectively. The variation of the time of melting and ablation with laser fluences is shown in Fig. 6(b).

Although simplifying the dynamics of the problem greatly, this simple model permits the calculation of melt times even when melt is not detectable. As long as ablation of the material is observable, and the laser fluence and thermal and optical parameters for the material are known, the melt time can be calculated.

It is evident from Fig. 6(a) that less energy is needed to ablate the target at higher CO_2 laser fluences. This may be explained on the basis of the high thermal conductivity of Zn. At the higher laser fluences, the rate of energy transfer from the laser to the target competes favorably with the loss of energy into the bulk due to diffusion. Therefore, at high fluences even a lower incident energy is more efficiently utilized in heating, melting, and subsequently ablating the target. The lower fluence counterparts suffer significant loss due to thermal diffusion and are relatively inefficient. This is consistent with the dissimilar results obtained in Part I of this series of articles, for similar studies done on ZnO.[1] There, the energy needed for melting ZnO at different CO_2 laser fluences was observed to be constant. In addition, a constant requirement of laser energy to cause ZnO to ablate was observed.[1] The explanation of this effect lies in the relatively poor thermal conductivity of ZnO. Its thermal conductivity is 0.29 W/cm K, which is 1 order of magnitude less than that of Zn.[3,4]

If we apply the model developed in this section to the case of ZnO, E'' in Eq. (1) should be zero since ZnO sublimes, and the latent heat of vaporization L_v does not exist. The parameter α in Eq. (1) is always equal to 1, and a theoretical calculation of the melt time is not necessary in this case. Actually, the melt time and the ablation time for a sublimating material are essentially the same. The differences in the observed times for melting and ablation for ZnO in Part I is explained on the basis of the finite propagation velocity of the molten layer on the ZnO surface (Sec. IV of Part I).

C. Particulate-free film growth of Zn

In this subsection we present the results of film deposition of Zn under dual-laser ablation using those CO_2 laser fluences consistent with the target reflectivity studies discussed in Sec. III B. Both the effects of CO_2 fluence and interpulse timing are addressed.

Once it became possible to determine the onset of the melt for Zn at different laser fluences on the basis of the transient reflectivity and the model calculations, a series of films were made. The different films were made on the low-jitter dual-laser ablation system, which has been discussed earlier. In our experiments, the KrF laser fluence was adjusted to 2.2 J/cm^2 which ensured that it was above the ablation threshold for Zn. The KrF laser spot size on the target was 9 mm^2 and spatially overlapped the CO_2 laser spot for the dual-laser ablated deposition. The films were deposited on room temperature Si substrates. Using CO_2 fluences of 5.85, 8.57, and 13.10 J/cm^2, the excimer laser pulses were temporally aligned with their respective calculated melt times. The results can be seen in Fig. 7. The scanning elec-

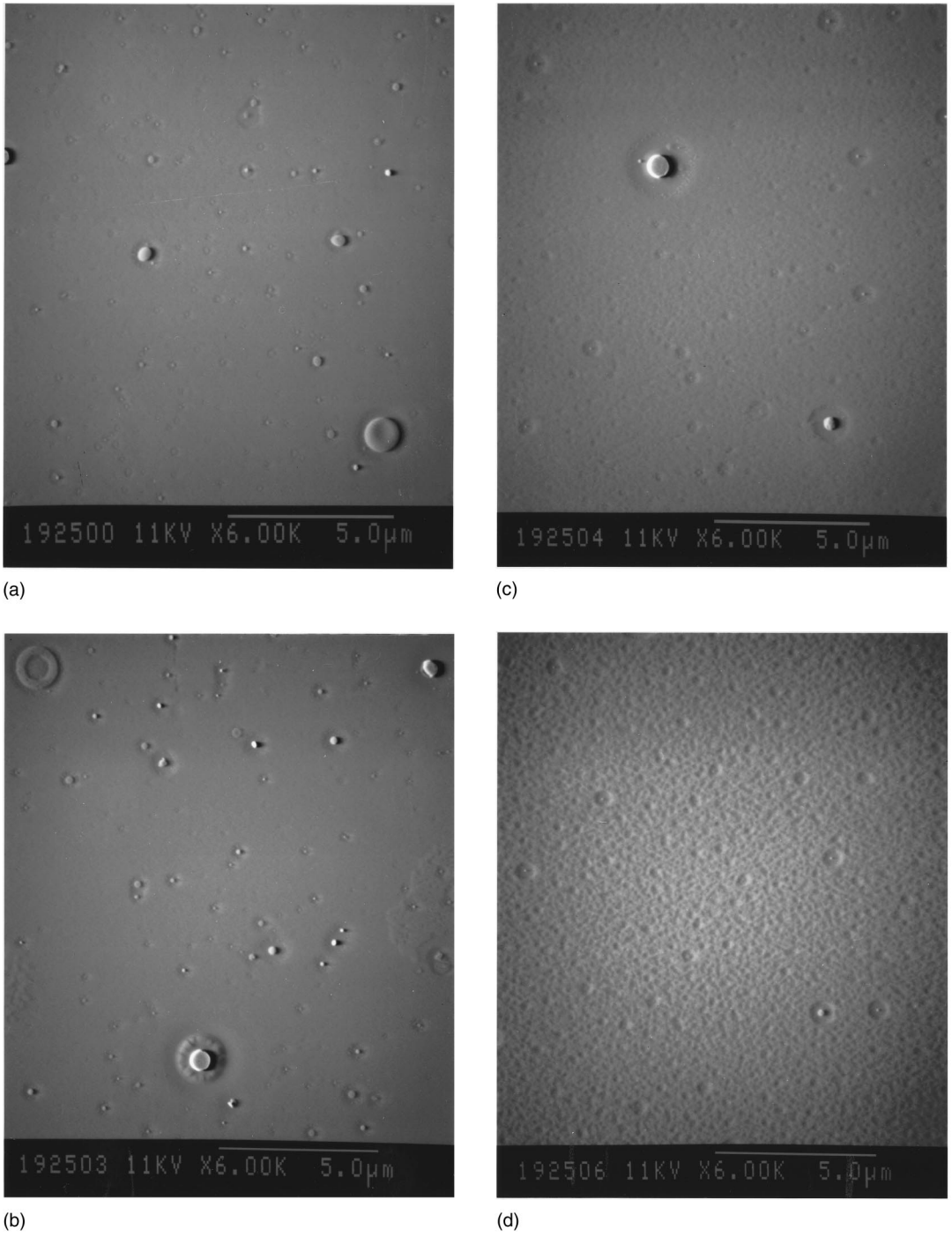

FIG. 7. SEM images of Zn films deposited with: (a) single laser ablation, and dual laser ablation at CO_2 laser fluences of (b) 13.10 J/cm^2, (c) 8.57 J/cm^2, and (d) 5.85 J/cm^2.

tron micrographs (SEMs) of the resulting films show a reduction in the size of particulates as the CO_2 fluence is reduced. If the fluence is too high, the CO_2 laser ablates the material along with the excimer laser. The number of large particulates has increased from Fig. 7(a) which is the single KrF laser ablation case, to the 13.1 J/cm^2 CO_2 fluence dual-laser ablation case shown in Fig. 7(b). There is also an increase in the number and size of both the micron and submicron particulates, which is expected with a laser-ablated film using a CO_2 laser.[8] As the CO_2 fluence is reduced, the size and density of the particulates drops [Fig. 7(c)], until there are substantially few visible particulates at a CO_2 fluence of 5.85 J/cm^2 under dual laser ablation [Fig. 7(d)].

In all of these films, the impact of the particulates clearly causes the formation of craters on the surface of the film. The lateral size and depth of the craters depend on the size of the deposited particulates. At the higher CO_2 laser fluences, although the particulate size and densities are larger, the background film is relatively smooth. As the CO_2 laser fluence is reduced, there is an increase in the overall surface roughness of the deposited films. This is due to the craters formed by a

higher density of submicron droplets at the lower CO_2 laser fluences. It is noteworthy that even though the CO_2 laser was adjusted to coincide with the onset of melt in each of the three dual-laser ablated Zn films, particulate-free films were not obtained at the higher CO_2 fluences. This emphasizes that even in dual-laser ablation the KrF ablated plume from a suitably molten target can be ineffective in screening the target from a high fluence CO_2 laser pulse. Therefore, both the timing and the CO_2 laser fluence play an important role in this particulate removal process.

At the high CO_2 laser fluences, the deposited particulates are dominated by large (greater than 1 μm) localized droplets. With a decrease in CO_2 laser fluence, there is a corresponding decrease in the size of these ''large'' droplets, resulting in a fluence regime in which they are disintegrated into finer droplets of larger number density. These droplets ($\sim$10–100 nm in size) create submicron craters over a proportionately larger film surface area, resulting in increased surface roughness. Reduction of the CO_2 laser fluence below 5.85 J/cm^2 for the deposition of Zn films should lead to both particulate removal and retention of surface smoothness of the films.

To demonstrate the importance of the interpulse delay and fluence, a series of films were deposited with a CO_2 laser fluence of 4.5 J/cm^2 and different interpulse delays (Fig. 8). It can be seen in Fig. 8(a) that when the excimer laser arrives before the CO_2 laser, there are a large number of particulates and they vary in size. Both surface roughness and particulate count are increased. A fairly high density of supermicron-sized particulates is observed, consistent with excimer ablation without premelting by the CO_2 laser. In the deposition of this film, both lasers ablated the target and the subsequent coupling of the CO_2 laser pulse into the plasma generated by the excimer pulse was inefficient in reducing the size of the large particulates. The CO_2 laser does cause an increase in the plasma temperature leading to ''splashes'' of large molten particulates impinging on the substrate. Figure 8(c) shows a film with lower particulate density, but there are still a number of micron-sized particulates. In this case, the CO_2 laser ablated the target, followed by the excimer laser. There was some coupling between the two laser pulses which reduced the number of submicron particulates from that observed in Fig. 8(a) to the case in Fig. 8(c). Also, the KrF laser does ablate from a molten target. However, the trailing edge of the CO_2 laser pulse (subsequent to KrF laser ablation) is ineffective in causing a substantial impact on the plasma temperature. This is consistent with no molten ''splashes'' being observed.

Clearly, the best film was obtained in Fig. 8(b) in which the particulates are absent. It is also noteworthy that at this reduced CO_2 laser fluence, the surface of the film is smooth, without the adverse effects of the minicraters observed in Fig. 7(d). The interpulse delay of 50–55 ns [in Fig. 8(b)] is consistent with the time expected for the onset of melt in Zn at a CO_2 laser fluence of 4.5 J/cm^2. This is based on extrapolating the calculated values based on the pump–probe experiments discussed in Secs. III A and III B [see, in particular, Fig. 6(b)].

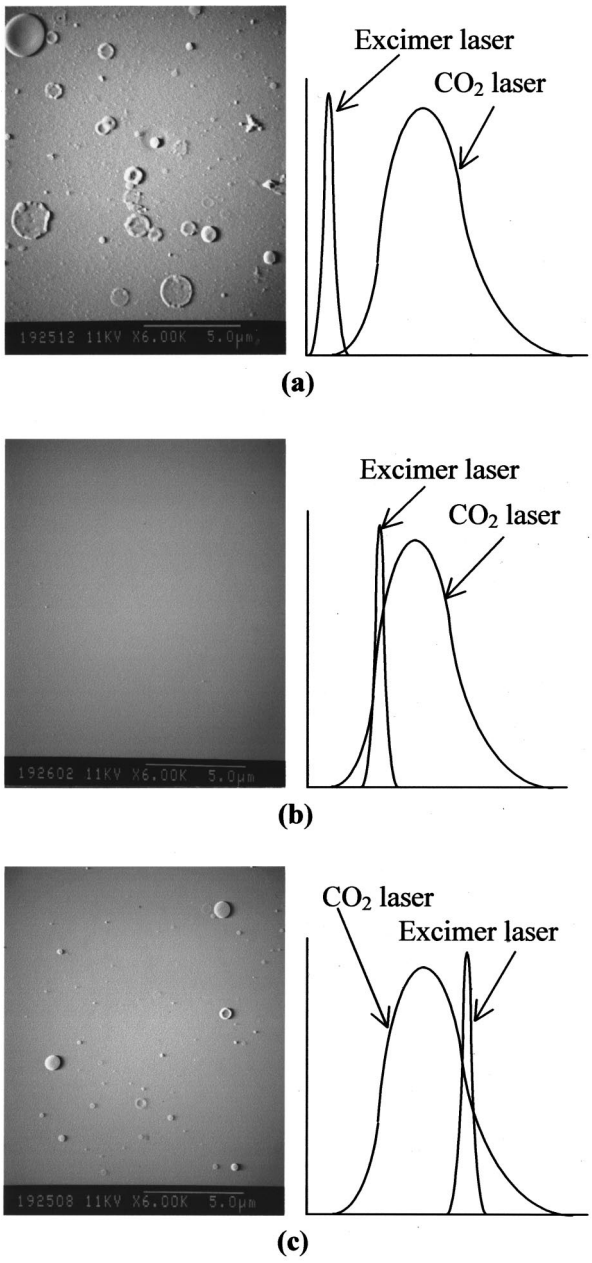

FIG. 8. SEM images of Zn films deposited using dual laser ablation at a CO_2 laser fluence of 4.5 J/cm^2, for a variety of corresponding interpulse delays that are represented in the figure. The time delay for the KrF laser in (b) is 50–55 ns after the onset of the CO_2 laser pulse.

IV. DISCUSSION AND CONCLUSIONS

In this paper, Part II, the transient target surface phase transformations under CO_2 laser irradiation including both melting and vaporization, have been observed for Mg and Al. These results made it possible to predict both the suitable CO_2 laser fluence and the interpulse delays in dual laser ablation that will result in particulate-free films of these metallic targets. Experiments to verify these specific predictions are currently in progress.

A new technique of single-shot transient reflectivity measurements incorporating a beam delay was introduced as a low-noise version of the single-shot configuration discussed in Part I.[1] This article also presented a simple thermal

model that was able to predict the onset of melt in a target of Zn for which the transient reflectivity was not able to detect the characteristic enhancement. The success of our approach in coupling the new probing technique (to determine the time of ablation of Zn) with a calculation of the time for the onset of melt by using the thermal model, was demonstrated by the deposition of particulate-free Zn films at the predicted interpulse delay. The critical role played by both the CO_2 laser fluence and the interpulse delay provided further direct evidence for our physical understanding of the particulate removal process in dual-laser ablation.

Most significantly, this series of two articles establishes directly both the physical basis and the technical approach using transient reflectivity measurements. This makes possible the universal deposition of particulate-free films of insulators and metals from packed-powder targets, reliably and reproducibly, by using suitably optimized dual laser ablation.

ACKNOWLEDGMENT

This research was supported in part by the National Science Foundation through Grant Nos. DMI-9622114, DMI-9978738, and DMI-0078917.

[1] P. Mukherjee, S. Chen, J. B. Cuff, P. Sakthivel, and S. Witanachchi, preceding paper, J. Appl. Phys. **91**, 1828 (2002).
[2] S. Witanachchi, K. Ahmed, P. Sakthivel, and P. Mukherjee, Appl. Phys. Lett. **66**, 1469 (1995).
[3] *Thermophysical Properties of Matter*, Thermophysical Properties Research Center, Purdue University (IFI/Plenum, New York, 1970).
[4] *CRC Handbook of Chemistry and Physics*, 62nd ed., Chemical Rubber Corp., Boca Raton, FL, (1981).
[5] E. Matthias, M. Reichling, J. Siegel, O. W. Kading, S. Petzoldt, H. Skurk, P. Bizenburger, and E. Neske, Appl. Phys. A: Solids Surf. **58**, 129 (1994).
[6] C. P. Grigoropoulos, in *Laser Ablation and Desorption*, edited by J. C. Miller and R. F. Haglund, Experimental Methods in the Physics Sciences (Academic, New York, 1998), p. 173.
[7] L. B. Pankratz, *Thermodynamic Properties and Oxides* (U.S. Dept. of the Interior, Bureau of Mines, Washington, D.C., 1982).
[8] J. T. Cheung, in *Pulsed Laser Deposition of Thin Films*, edited by D. B. Chrisey and G. K. Hubler (Wiley, New York, 1994), pp. 1–22.